ELSEVIER

Journal of Hazardous Materials A79 (2000) 41–61

Journal of Hazardous Materials

www.elsevier.nl/locate/jhazmat

Comparison of a reduced explosion model to blast curve and experimental data

J. Keith Clutter [a,*], Robert T. Luckritz [b]

[a] *Analytical and Computational Engineering, Inc., P.O. Box 809, Helotes, TX 78023, USA*
[b] *QAnalytics, Mountain Lakes, NJ, USA*

Received 10 November 1998; received in revised form 13 February 2000; accepted 16 February 2000

Abstract

This paper discusses a new reduced model for vapor cloud explosions (VCEs) which incorporates some factors found in more complex models such as three-dimensional effects. The common foundation of all VCE analysis models is discussed and a simplified model based on a set of blast curves is reviewed to highlight the differences in the various model assumptions. Output from the reduced model is compared to experimental data and results from the simplified model. It is shown that the reduced model captures critical factors such as cloud shape and flame dynamics.

Keywords: Reduced explosion model; Blast curve; Cloud shape; Flame dynamics; Vapor cloud explosions

1. Introduction

Accidental vapor cloud explosions (VCEs) remain a primary concern for the petrochemical industry and many facets of the explosion problem must be addressed. These issues range from the probability of an explosion occurring to determination of the possible consequences of such an event. Here, the focus is on models useful in predicting these consequences. Before discussing details of the specific models to be studied here, general classifications of explosion models are defined.

At one end of the modeling spectrum are analysis tools which incorporate the exact three-dimensional characteristics of the facility involved in the explosion as well as the

* Corresponding author. Tel.: +1-210-862-1481; fax: +1-210-681-1482.
E-mail address: clutter@aceng.net (J.K. Clutter).

0304-3894/00/$ - see front matter
PII: S0304-3894(00)00185-0

physical and chemical phenomena involved. These tools allow for incorporation of aspects such as the vapor cloud shape, ignition location and presence of structures. Examples of such models are FLACS [1] and EXSIM [2].

The complex models solve a full set of partial differential equations governing fluid dynamics as well as equations governing the combustion process. These equations are solved at several points in the domain of interest. The combustion process is typically represented by a single-step chemical reaction and the progression of the reaction is dictated by local conditions including turbulence. In addition, the complex analysis tools also model the plant facility in high detail. For instance, each vessel and pipe located in the facility can be input into the computer model. Such objects influence the flow, generate turbulence and affect blast propagation.

At the other end of the modeling spectrum are simplified models which use a set of data generated for an idealized explosion scenario. Examples of this class include the Multi-Energy and Baker–Strehlow methods [3]. Here a single-cloud shape (i.e. hemispherical or spherical), ignition location, and cloud composition are used. In some cases, the basis for the model has been generated with numerical codes that solve a set of partial differential equations similar to those solved by the complex models. The combustion process is incorporated by an energy additional term and the rate of the reaction progression is determined by an assigned flame speed. When this class of model is used in determining VCE consequences, details such as cloud shape, local stoichiometry, and physical obstacles are not explicitly incorporated. Some aspects such as local congestion and confinement are included empirically. A review of several simplified models is provided by Lees [3] and more details on one of the simplified models to be used here are provided later.

The third class of analysis tools discussed here falls between the complex and simplified models. This class is labeled reduced to emphasize that they do not incorporate all the features found in the complex models and yet they display more details than the simplified models. This class solves nearly the same set of partial differential equations as the complex models, differing only in some of the physical phenomena representations. In this class of models, there is no explicit equation for turbulence. The rate of reaction is based on empirical data but the combustion process is represented by a single-step chemical reaction as in the complex models.

The reduced models do include cloud shape and ignition location. Major structural components can be included to predict blast propagation, focusing, and shielding. However, the reduced model does not include every process item such as each individual pipe.

2. Governing equations

The chemically reacting flow in a VCE is governed by the Navier–Stokes equations with additional equations for the reaction process. These include continuity,

$$\frac{\partial}{\partial t}(\rho) + \frac{\partial}{\partial x_j}(\rho u_j) = 0, \tag{1}$$

and momentum,

$$\frac{\partial}{\partial t}(\rho u_i) + \frac{\partial}{\partial x_j}(\rho u_i u_j) + \frac{\partial P}{\partial x_i} = + \frac{\partial}{\partial x_j}(\tau_{ij}) + \rho g_i \tag{2}$$

where u_i is the velocity in the x_i direction, P is pressure and ρ is density. The shear stress in the ith direction on a surface normal to the jth direction is represented by τ_{ij} and g_i represents a body force in the ith direction.

The energy equation is

$$\frac{\partial}{\partial t}(\rho E) + \frac{\partial}{\partial x_j}(\rho u_j H) = -\frac{\partial}{\partial x_j}(J_{h,j}), \tag{3}$$

where $H = E + P/\rho$, $E = e + (1/2)\vec{u}^2$ and e is internal energy. The diffusion of enthalpy in the jth direction is represented by the term $J_{h,j}$. The internal energy is related to the individual species enthalpy (h_i) through the relationship

$$e = E - \frac{1}{2}\vec{u}^2 = \sum_{i=1}^{\mathrm{NS}} \alpha_i h_i - \frac{P}{\rho} \tag{4}$$

where

$$h_i = h_{\mathrm{f}_i}^0 + \int_{T_\mathrm{R}}^{T} \mathrm{Cp}_i \mathrm{d}T \tag{5}$$

with Cp_i and $h_{\mathrm{f}_i}^0$ being the specific heat at constant pressure and the heat of formation of species i, respectively. A species continuity equation of the form

$$\frac{\partial}{\partial t}(\rho \alpha_n) + \frac{\partial}{\partial x_j}(\rho \alpha_n u_j) = -\frac{\partial}{\partial x_j}(J_{n,j}) + \dot{\omega}_n \tag{6}$$

is needed for each species involved in the combustion process. The term α_n is the mass fraction of species n, varies between 0 and 1 and is nondimensional. The mass diffusion of species n is represented by $J_{n,j}$ and $\dot{\omega}_n$ is the chemical reaction source term for the species.

Viscous effects are manifested through the shear stress term, τ_{ij}, and diffusion terms $J_{h,j}$ and $J_{n,j}$ which are dependent on viscosity, μ. The effective viscosity is a sum of laminar and turbulent quantities,

$$\mu = \mu_\mathrm{L} + \mu_\mathrm{T}. \tag{7}$$

The turbulent contribution is related to the turbulent kinetic energy (k) and the dissipation of this energy (ε). Explicit inclusion of turbulence using k and ε requires the solution of at least two more equations [4].

In the most general of terms, the reaction process is composed of NS total species and NR total reactions expressed in the form

$$\sum_{j=1}^{\mathrm{NS}} \nu'_{ij} X_j \underset{k_{\mathrm{b}_i}}{\overset{k_{\mathrm{f}_i}}{\rightleftarrows}} \sum_{j=1}^{\mathrm{NS}} \nu''_{ij} X_j, \qquad i = 1, \ldots, \mathrm{NR} \tag{8}$$

and the source terms is in the form

$$\dot{\omega}_n = M_n \sum_{i=1}^{\mathrm{NR}} (\nu''_{in} - \nu'_{in}) \times \left(k_{f_i} \prod_{j=1}^{\mathrm{NS}} X_j^{\nu'_{ij}} - k_{b_i} \prod_{j=1}^{\mathrm{NS}} X_j^{\nu''_{ij}} \right) \tag{9}$$

where M_n is the molecular weight of species n. Here ν'_{ij} and ν''_{ij} are the stoichiometric coefficients for species j in reaction i, and X_j is the molecular concentration of species j. The parameter k_{f_i} and k_{b_i} are the forward and backward reaction rates. The representation of the reaction process as well as the diffusion of species and the shear stress are needed for simulating VCE problems. It is the exact form of these representations that distinguish the various model classes as discussed next.

3. Complex models

In the complex class virtual representations of the facility are constructed explicitly including components such as walls, piping, and vessels. Large objects can obstruct the flow and shield some areas from the blast while focusing blast into other areas. Small objects such as piping generate turbulence and are usually represented through a sub-grid scale obstruction model [5]. The sub-grid model is incorporated into the various governing equations; one example can be found in Ref. [2].

In the complex model, the combustion process is represented as a single-step, irreversible reaction of the form

$$\mathrm{F} + \mathrm{O} \rightarrow \mathrm{Pd} \tag{10}$$

involving the fuel (F), oxidizer (O), and product (Pd). The source term of Eq. (6) for the fuel, expressed based on the general form of Eq. (9) would be

$$\dot{\omega}_{\mathrm{F}} = -k_{\mathrm{f}} M_{\mathrm{F}} (X_{\mathrm{F}} X_{\mathrm{O}}) \tag{11}$$

where k is the rate of the reaction for the irreversible process. The combustion is dependent on the molecular concentration of fuel and oxidizer and in areas where the concentration of fuel and oxidizer approaches zero, the combustion process drops to zero. This is how air-limited and fuel-limited combustion is represented. The reaction rate is dependent on local conditions such as temperature.

The complex models use a format similar to Eq. (11) such as

$$\dot{\omega}_{\mathrm{F}} = -\beta \frac{u_{\mathrm{L}}}{\delta_{\mathrm{L}}} \rho \alpha_{\mathrm{lim}} \tag{12}$$

where β is an enhancement factor that incorporates local turbulence effects such as flame wrinkling. This is applied to the laminar burning velocity (u_{L}) and laminar flame thickness (δ_{L}) which are dependent on the fuel–oxidizer mixture and are proportional to the reaction rate ($k \propto u_{\mathrm{L}}/\delta_{\mathrm{L}}$) [6]. The enhancement factor is coupled to the other equations through the turbulent viscosity and flame characteristics, $\beta = \beta(\mu_{\mathrm{T}})$. The dependence on fuel and oxidizer concentration in Eq. (11) is represented in Eq. (12) through the parameter α_{lim} which is set equal to the smallest mass fraction among all species involved in the reaction.

When Eq. (12) is compared to Eq. (11), it is clear that the enhancement factor and laminar combustion characteristics of the mixture combine to give an effective reaction rate (k_e) and the source term takes the form

$$\dot{\omega}_F = -k_e \rho \alpha_{\lim}. \tag{13}$$

The complex models utilize a high fidelity model of the fluid dynamic and reactions processes. These models are able to exactly represent the shape and composition of the vapor cloud and the ignition location. Typical vapor clouds are formed in large, pancake shapes. When such a cloud is involved in an explosion, the resulting energy release can easily escape through the large surface area bounding the top of the cloud. This prevents any feedback processes such as precompression of unburned gases ahead of the flame and results in explosions much less severe than if the cloud was in a spherical or hemispherical shape.

Furthermore, in the explosion process, pressure buildup will push the vapor cloud out of congested regions and as the flame exits these congested regions, the flame speed drops off substantially. Therefore, the total energy added during the explosion is much less than if all the vapor cloud initially in the congested regions contributed to the VCE. The complex models have the ability to include these factors into the prediction of the explosion. However, they are not yet widely used, partly because they can require large amounts of time to construct the virtual representation of the facility.

4. Simplified model

The simplified model included in the current study is the Baker–Strehlow method. As Lees [3] reports, this method is based on numerical studies conducted by Luckritz and Strehlow et al. [7,8]. Further information on this model can be found in Refs. [9–12]. Luckritz studied the combustion of spherical vapor clouds and the effect of flame speed on the pressure and impulse generated during the VCE process. Some of the results found in Ref. [7] are the pressure and impulse curves shown in Figs. 1 and 2. Pressure and impulse are functions of a scaled distance, $R(P_0/E)^{1/3}$, from the cloud center where E denotes the total energy of the vapor cloud, P_0 the ambient pressure and a_0 the corresponding ambient speed of sound. The flame speed (M_w) is a second parameter determining the explosion output.

In this earlier work, Luckritz used a Lagrangian frame of reference to solve the governing equations in a spherical coordinate system. This results in a one-dimension solution where quantities vary only with radius (R). The equations solved include a conservation equation for mass, momentum, and energy but no additional equations for species. Viscous effects and turbulence are neglected. Luckritz's model represents the combustion process with an addition term in the energy equation, converting Eq. (3) to

$$\frac{\partial}{\partial t}(\rho E) + \frac{\partial}{\partial x_j}(\rho u_j H) = \Lambda, \tag{14}$$

where Λ is the energy addition term. Spatial and temporal variation is given by $\Lambda = \lambda_1(r)\lambda_2(r,t)$. A cosine function was used by Luckritz to smoothly vary the term

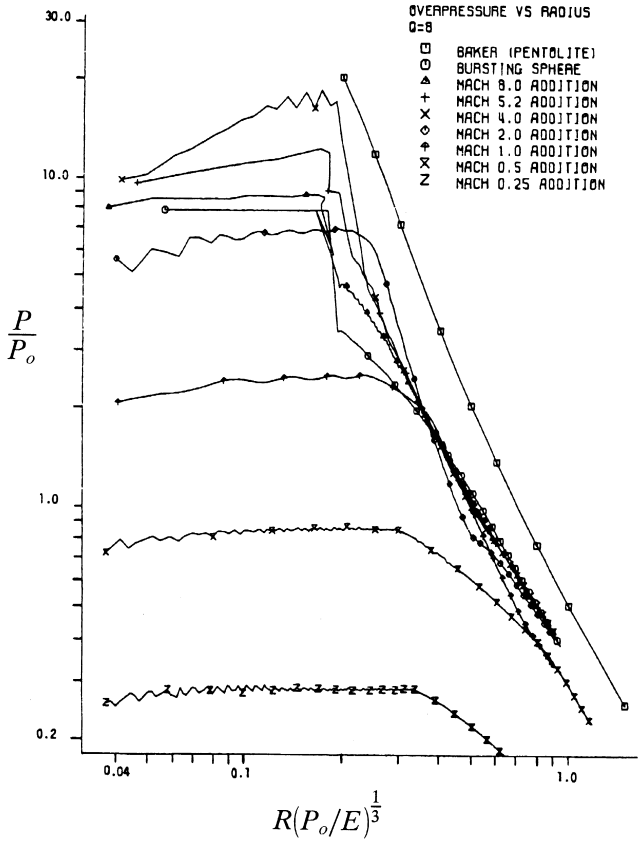

Fig. 1. Overpressure versus scaled distance calculated by Luckritz.

$\lambda_1(r)$ from 1 to 0 at the edge of the vapor cloud. The amount of energy is set by the term $\lambda_2(r,t)$ which varies from 0 to Q, the maximum amount of energy released determined by the fuel involved. The worst explosion will occur with a stoichiometric mixture in the cloud and Luckritz [7] presents values for a range of fuels. In his simulations a value of $Q = 3.508$ MJ/kg is used to mimic the characteristics of a stoichiometric methane–air cloud.

The function λ_2 is related to assumed flame dynamics. Flame width is measured by the time required for the flame to pass a specific point (τ_C). Luckritz simulates various flame widths but the majority of data presented in Ref. [7] (and that shown here in Figs. 1 and 2) uses a flame width such that $\tau_C/\tau_T = 0.1$ where τ_T is the time required for the flame to reach the edge of the cloud. Using the flame arrival time (τ_A) and the passage time (τ_C) at each point in the cloud, the energy function is expressed as

$$\lambda_2 = \begin{cases} 0, & t \le \tau_A \\ Q', & \tau_A < t \le \tau_A + \tau_C \\ Q, & t > \tau_A + \tau_C \end{cases}. \tag{15}$$

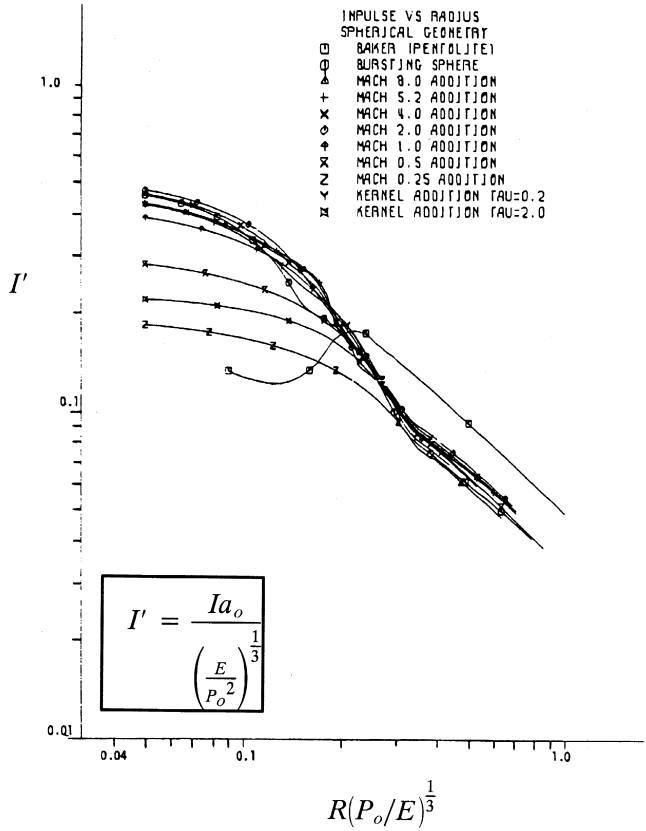

Fig. 2. Scaled impulse versus scaled distance calculated by Luckritz.

A cosine function, over a quarter of a period, is used to vary Q' from 0 to Q. This is depicted in Fig. 3 and was used to closely mimic the model by Zajac and Oppenheim [13]. The arrival and passage times are akin to combustion time scales such as induction and reaction times which Clutter [4] has shown impacts the pressure generated during the reaction process.

In complex models, transformation from reactants to products during combustion is handled through the continuity equations for each species. In Luckritz's model this process is represented by altering the value of the specific heat ratio, γ, in the equation of state. In Ref. [7], the specific heat ratio is 1.4 before the arrival of the flame and 1.2 once the flame has passed. The variation between 1.4 and 1.2 is coupled to the energy release function of Eq. (15) by

$$\gamma = 1.4 - 0.2(\phi) \tag{16}$$

where ϕ is the fraction of energy that has been released. He assumes that the molecular weight stays constant at a value equal to that of air. This is a reasonable assumption since a large quantity of nitrogen is present in the stoichiometric cloud.

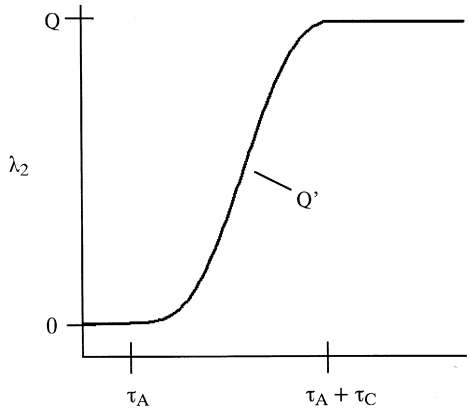

Fig. 3. Depiction of energy addition function.

For simplified models such as that of Luckritz, all factors such as turbulence and flame curvature, which affect the rate of combustion, can be considered to be embodied in the parameter M_w. The velocity of the flame is a result of the balance between the reaction and diffusion processes [14]. Following this idea, Baker et al. [9] present tables correlating various combinations of fuel reactivity, confinement, and obstacle density to M_w. These correlations are based on a survey of experiments in which flame speeds were recorded for various confinement and obstacle configurations [10]. Thus, even though effects such as turbulence and flame curvature are not explicitly included in the model, they are represented in M_w.

The final aspect of the simplified model is a determination of the effective portion of the vapor cloud involved in the explosion [3]. Unlike the complex models, the Baker–Strehlow Method does not include a calculation of that portion of the cloud that is pushed out of congested regions during the explosion process. Therefore, typically the entire cloud occupying areas such as a process units prior to the explosion, are assumed to contribute.

Some key aspects of the VCE problem are ignored with simple models, including the effect of cloud shape. The Baker–Strehlow method uses a set of curves from spherical clouds that can give blast pressures higher than typical pancake shaped clouds formed in releases. Therefore, the Baker–Strehlow results will typically be very conservative. Furthermore, omitting cloud movement and shielding effects in the simple models contributes to conservative predictions. However, neglecting focusing can give lower than actual overpressures.

5. Reduced model

Clutter [16] has developed a new Computational Explosion and Blast Assessment Model (CEBAM) which is a reduced model. The reduced model solves a three-dimensional set of equations for three species, a reactant mixture (Rx), combustion products (Pd), and ambient air (Air). The specific heat for each species is assumed constant at the

Table 1
Species and properties used in the reduced model

Species	Symbol	Cp/R_u	h_f (kcal/mol)
Reactant	Rx	3.5	0
Product	Pd	6	−24.19
Ambient air	Air	3.5	0

values in Table 1 with R_u being the universal gas constant. These values were selected to reproduce the values of γ used in Luckritz's model, Eq. (16). The specific heat at any point in the field is found as

$$Cp = \sum_{i=1}^{NS} \alpha_i Cp_i. \tag{17}$$

The molecular weights for all species were set to be equal to that of air. The heat of formation for each species given in Table 1 generates the same amount of energy release as that used in Luckritz's earlier model.

As in the complex models, the combustion process is represented with a one-step, irreversible reaction of the form

$$Rx \rightarrow Pd. \tag{18}$$

The reduced model has the ability to represent the fuel and oxidizer explicitly, however, here Rx represents a stoichiometric mixture of fuel and oxidizer to follow Luckritz's

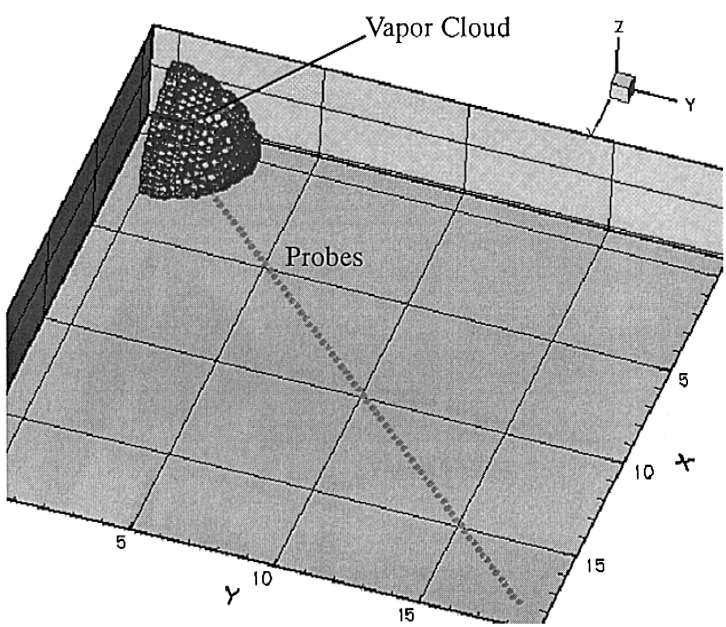

Fig. 4. Domain and initial vapor cloud used in VCE simulations.

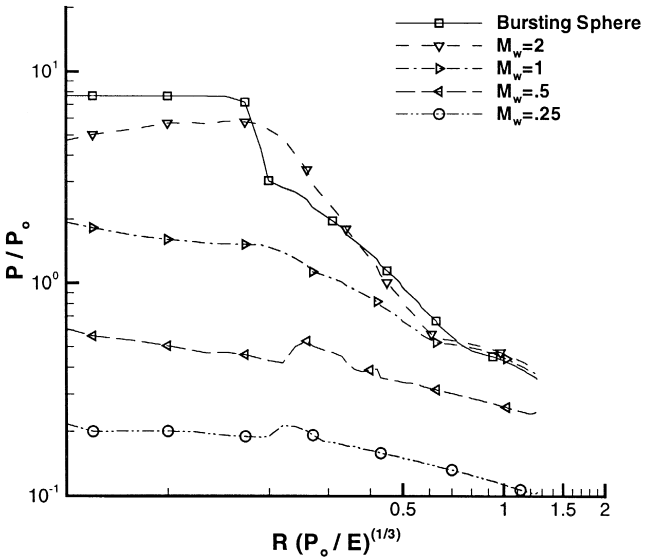

Fig. 5. Overpressure computed with CEBAM versus scaled distance.

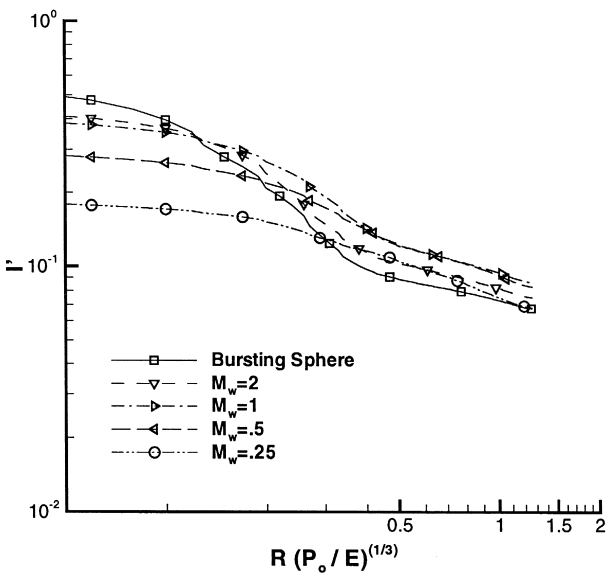

Fig. 6. Impulse computed with CEBAM versus scaled distance.

Table 2
Summary of small-scale EMERGE tests

Test no.	Mixture	Max. V_f (m/s)	P_{max} inside (kPa)	P_{max}, $x = 3.06$ m (kPa)	P_{max}, $x = 5.33$ m (kPa)	P_{max}, $x = 10.7$ m (kPa)
7	M	52	6.9	2.1	1.2	0.6
8	M	52	6.7	2	1.2	0.6
10	M	70	7.7	2.4	1.3	0.7
28	M	127	30.7	13.3	7.9	4.6
29	M	93	29.4	11.5	6.6	3.3
30	M	107	25	9.7	5.7	2.9
31	M	107	26.4	11.3	6.4	3.5
33	M	130	24.3	9.1	5.2	
34	M	106	28.6	12.2	7.1	3.6
15	P	52	10.2	3.3	1.8	0.9
16	P	74	9.9	2.9	1.7	0.8
40	P	208	57.8	27.4	16.8	8.3
41	P	179	51.7	23	13.5	6.9
42	P	163	55.5	25.5	15	7.3
50	P	280	54.2	24.6	14.7	7.3
52	P	217	51.7	23.9	14.5	7.2

earlier work. Two different models for reaction rate and initiation were tested. First constant flame speeds are assumed to determine if the new model can reproduce the earlier results of Luckritz [7].

5.1. Constant flame speed model

For the reduced model, the viscous terms are not included in the set of equations solved. Turbulence variations are represented by varying flame speed. Each computational cell is assigned an arrival or activation time (τ_A) based on the flame speed. The

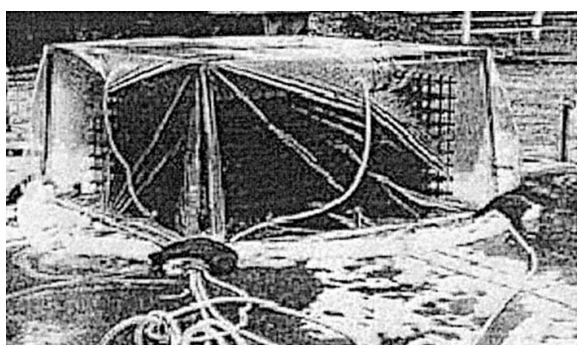

Fig. 7. Experimental configuration used in the EMERGE tests.

reaction rate is related to the time it takes the flame to pass through a given computational cell (τ_C). The initial conditions in the cloud are $\alpha_{Rx} = 1$ and the concentration of reactants reaches 0 once the flame passes to reproduce the results of Luckritz's model. Therefore, the effective reaction rate is $k_e = 1/\tau_C$ which results in a source term for the reactant mixture in cell *i,j,k*

$$\dot{\omega}_{Rx} = -k_e \rho \alpha_{Rx} = -\rho \alpha_{Rx}/\tau_C \tag{19}$$

where α_{Rx} is the mass fraction of the reactant mixture.

In the reduced model, with the addition of the species continuity equations, any convection of reactants out from the initial boundary are modeled. This deviation from a condition of $\alpha_{Rx} = 1$ will result in a reduction in the amount of energy added at the boundary of the expanded cloud.

5.2. Decelerating flame speed model

An alternative flame speed model uses the same framework as the model described above with one alteration to account for the fact that generated turbulence varies with

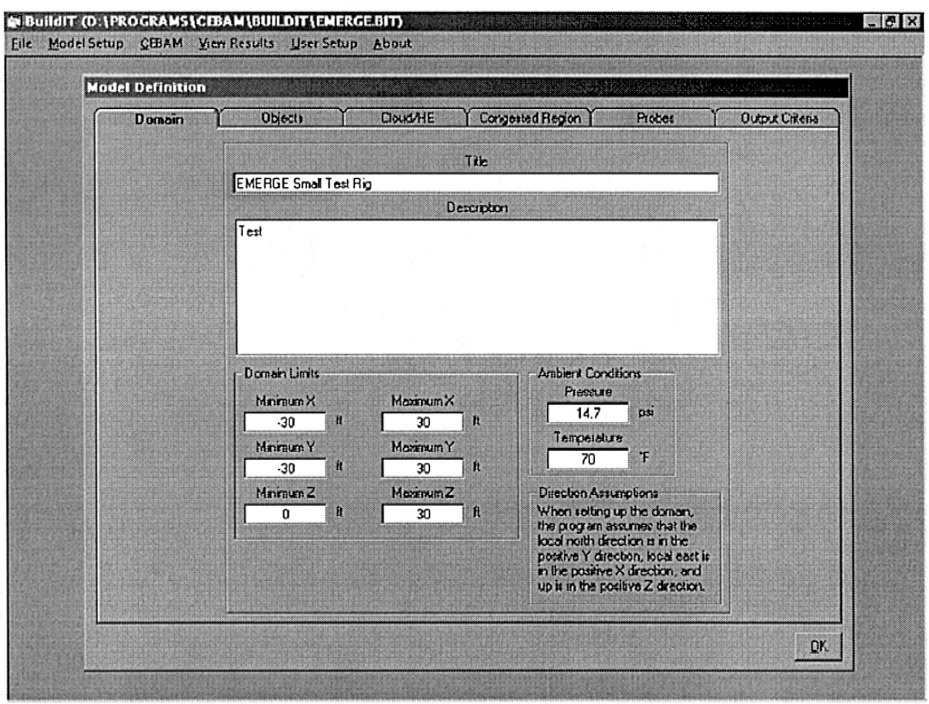

Fig. 8. GUI screen for defining the computational domain.

location. This flame speed model takes advantage of the three-dimensional framework of CEBAM to designate the variation in local conditions. Vacant regions surrounding areas of congestion are designated to have flame speed values of essentially zero. Bordering the congested regions, the flame speed decelerates linearly from a maximum value to zero. The local reaction rate is set based on the flame speed.

5.3. Inclusion of facility aspects and cloud parameters

The role of large and small objects have been mentioned previously and these effects are incorporated in CEBAM as follows. Key objects such as buildings and large vessels are explicitly represented. However, piping runs and sections of process units are represented simply as areas of congestion. CEBAM uses the empirical correlations found in Refs. [9,10] to set the flame speed in these defined congestion zones. This sets the effective reaction rate (k_e). This approach dramatically reduces the model definition time to only a matter of minutes.

CEBAM also allows for the representation of the exact cloud shape and ignition location. A correct representation of how much of the vapor cloud is driven out of the congested regions is also made.

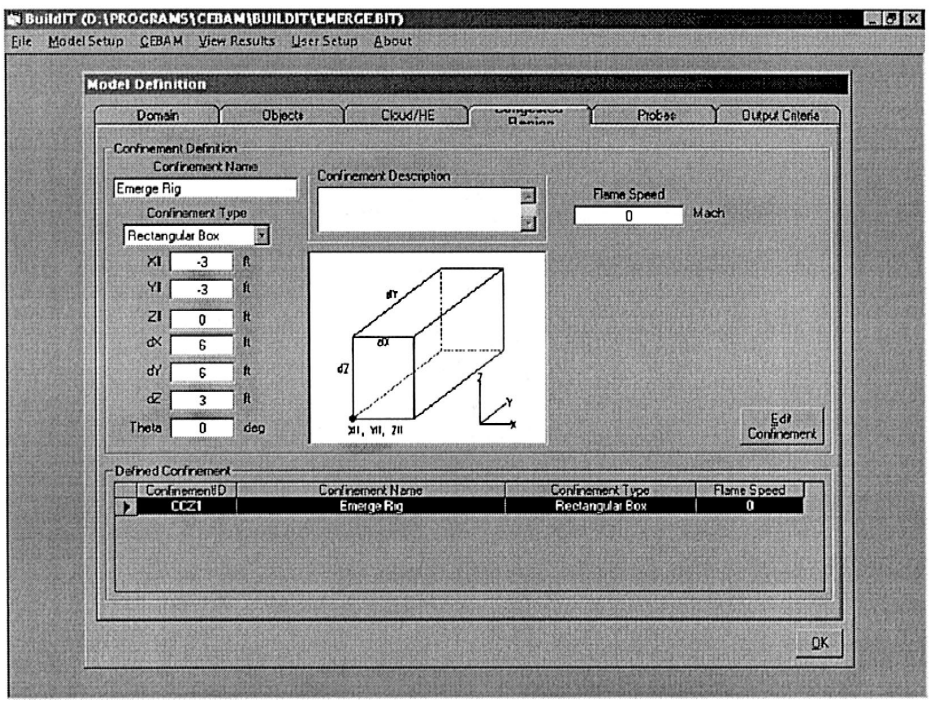

Fig. 9. GUI screen for defining areas of congestion.

5.4. Solution of governing equations in CEBAM

CEBAM uses a finite volume formulation within a curvilinear framework for solution of the equations. A flux-vector splitting scheme with variable extrapolation is used along with a predictor-corrector method to achieve 2nd order in time and space. An operator splitting routine described in Refs. [4,17] is also used to increase computational efficiency.

6. Results comparing the reduced and simplified model

A spherical vapor cloud is simulated first to mimic the earlier study of Luckritz [7]. Here this scenario is simulated using the reduced model with the conditions shown in Fig. 4. Only 1/8th of the domain is solved and three planes of symmetry are employed to reduce the required computational resources. Fig. 4 shows the initial location of the cloud which is composed of the reactant mixture, Rx. Also shown are locations where pressure time histories are recorded to determine peak pressure and impulse.

The amount of energy release through the formulated 3-fluid model is compared to the earlier results by setting the reaction time to 0 as assumed by Luckritz [7] to produce the bursting sphere curve in Figs. 1 and 2. The results in Figs. 5 and 6 show that using the heat of formations of Table 1 produces the same amount of energy released as that

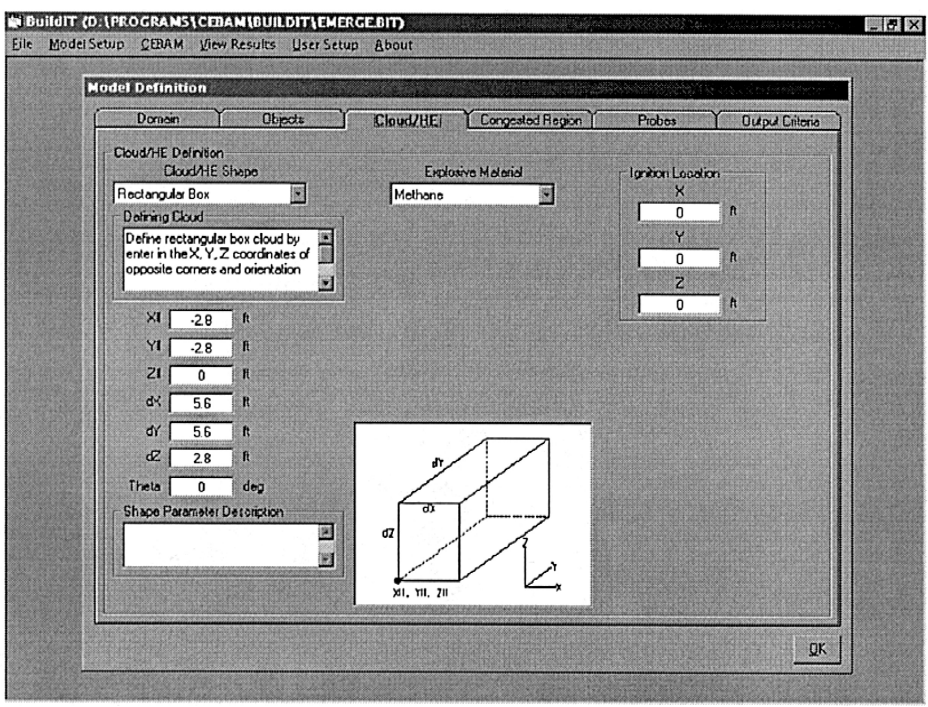

Fig. 10. GUI screen for defining vapor clouds and ignition location.

used in Ref. [7]. The remaining simulations used the condition $\tau_C/\tau_T = 0.1$ mentioned earlier.

Various constant flame speeds are used coinciding with the values presented in Ref. [9] that relate to experimental data. The curves of Figs. 5 and 6 compare well with the early results of Luckritz [7] both in magnitudes and variation with scaled distance. The current results include values at scaled distances smaller than those of Luckritz [7] and in this region the current results show an increase in peak pressure.

7. Results comparing the reduced model to experimental data

CEBAM, using the two flame speed assumptions, is compared to experimental data from the Extended Modeling and Experimental Research into Gas Explosions (EMERGE) Project. This project measured overpressures at various distances from explosions in rectangular configurations of pipes. Experiments were conducted for small, medium, and large configurations with a variety of fuels [18]. Here, the data for the small tests using methane and propane are used and provided in Table 2.

Fig. 7 shows a picture of the medium sized test rig used in the experiments. The small rig configuration was similar and sized 6 ft by 6 ft by 3 ft tall. The rig was surrounded by a tent to contain the vapor cloud and the ignition location was set at the center of the rig, on the ground. The available data from the test are the measured flame

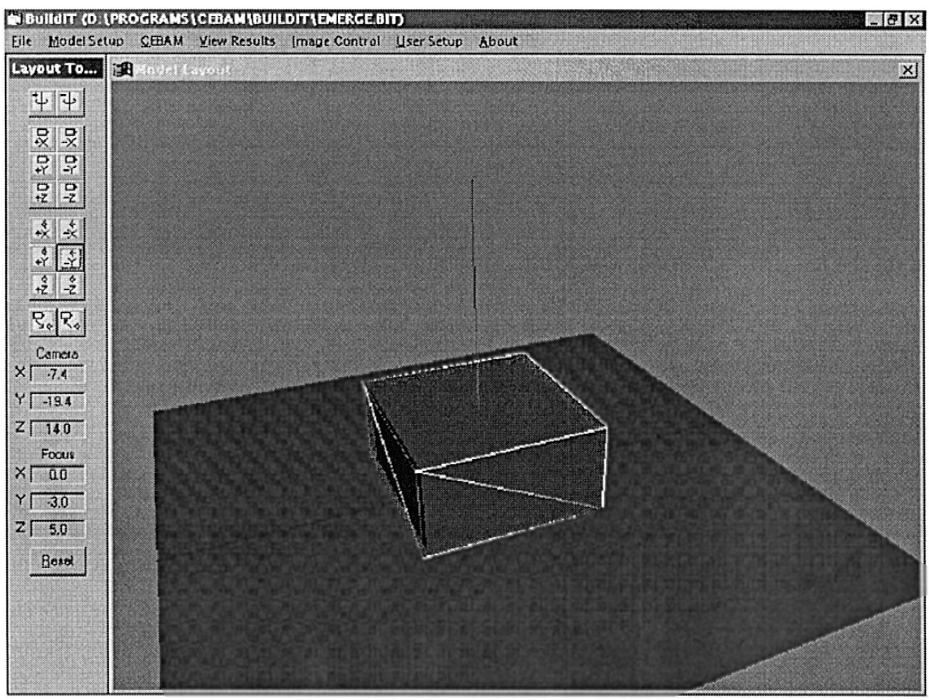

Fig. 11. GUI screen showing the defined explosion scenario.

speed and the overpressure at three locations outside the rig as well as the average overpressure in the rig.

Simulations are made using CEBAM for the rectangular configuration of the EMERGE tests and Fig. 8 shows the graphical user interface (GUI) input which defines the domain of interest. The screen of Fig. 9 allows for the definition of the congestion zones. This is followed by the definition of the vapor cloud and the ignition location using the GUI screen of Fig. 10. Both the congestion zones and vapor cloud can be defined in a multitude of shapes but here both are rectangular. There are also tabs for the definition of objects, probes, and the output criteria. The object definition option can be used to specify structural elements such as walls, floors, etc. and to assign specific failure criteria to these items. However, for the EMERGE configuration here, no objects are involved. Fig. 11 shows the complete CEBAM representation of the experiments.

The experimental data for the methane case can be grouped into two average flame speeds of Mach Numbers $M_w = 0.17$ and 0.32, relative to ambient conditions. Simulations at these speeds, using the combustion model of Luckritz, are shown in Figs. 12 and 13 and labeled *rect*. This is to denote these results incorporate only the rectangular shape effects associated with the test configuration since the combustion proceeds until all the vapor cloud has been consumed. This is true even if the overpressure build-up pushes the reactant mixture out of the congested region. The experimental data are represented with the solid symbols. Even though the exact cloud shape is used, the combustion model causes an overprediction of the blast pressure at locations outside the rig.

Here, the energy scaling for distance is not used. As noted by Lee et al. [15], for realistic scenarios, energy scaling is not appropriate because the actual amount of energy

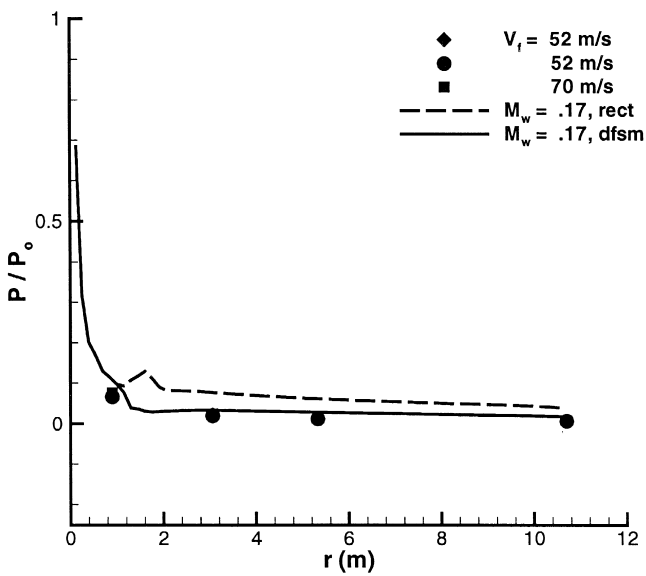

Fig. 12. Results for the $M_w = 0.17$ case showing the rectangular (rect) configuration and the decelerating flame model (dfsm).

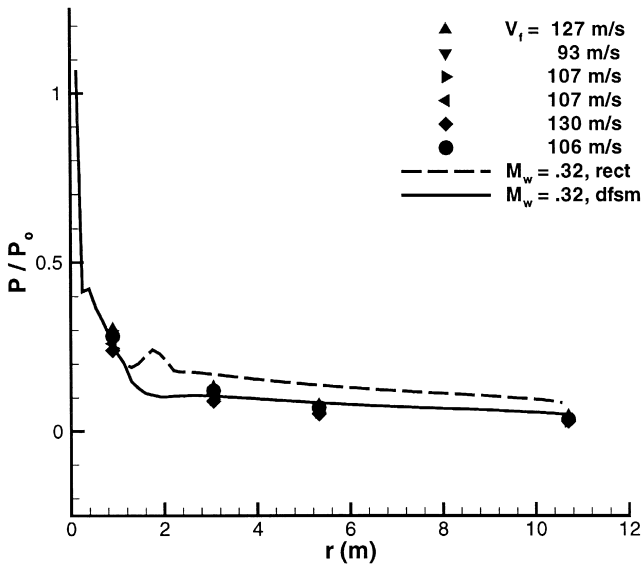

Fig. 13. Results for the $M_w = 0.32$ case showing the rectangular (rect) configuration and the decelerating flame model (dfsm).

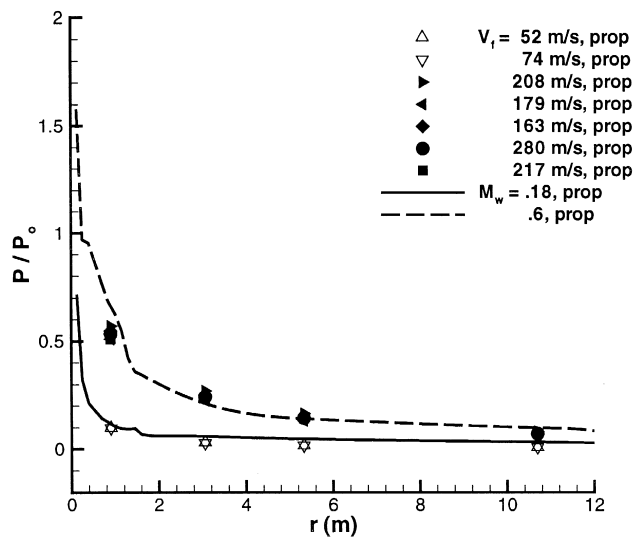

Fig. 14. Results for the stoichiometric propane–air cases using the decelerating flame model.

involved in the explosion process cannot be assessed a priori. Lee et al. attribute this to the fact that the detailed blast flow structure must be known to make accurate assessments of the total energy involved. Ad hoc functions can be applied to the spherical data to estimate the expansion of the cloud during the explosion but such functions would be highly dependent on the exact layout of the facility in which the explosion occurs.

Next, computations are made using the rectangular cloud shape found in the experiments and the decelerating flame speed model. For the small scale experimental configuration, it is assumed that the flame decelerates from the constant value defined for the specific congestion of the rig to zero over a distance approximately equal to 15% of the width of the rig. Universal applicability of this value is not proposed. It is used here to demonstrate how inclusion of flame deceleration affects the computed explosion output. These results are also in Figs. 12 and 13 and labeled *dfsm*. By simulating the deceleration of the flame outside the rig, the overpressure is more accurately predicted.

The data from the small-scale EMERGE tests for a stoichiometric propane–air mixture can be grouped into two average flame speeds of $M_w = 0.18$ and 0.6. For these cases, only the decelerating flame speed model is used and the comparison is shown in Fig. 14. Using CEBAM with this model, good predictions of the overpressures are made at locations in and outside the rig.

8. Comparison of the simplified model to experimental data

Here the Baker–Strehlow Method is used for the conditions of the EMERGE small-scale cases to further compare the simplified and reduced classes of models. The

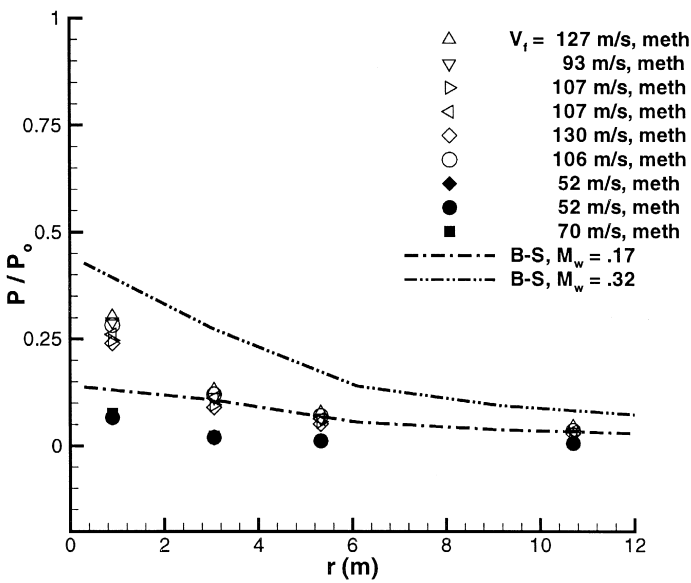

Fig. 15. Results for the small-scale EMERGE methane cases from the simplified model.

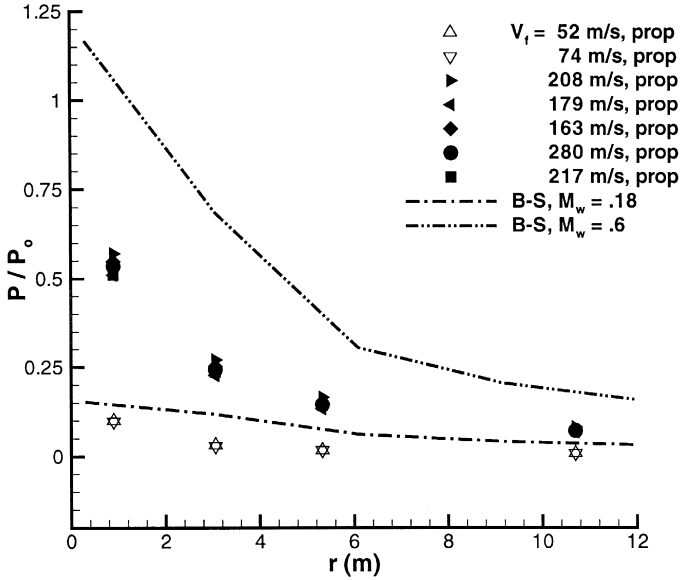

Fig. 16. Results for the small-scale EMERGE propane cases from the simplified model.

original curves from Luckritz [7] were later augmented by Stehlow et al. with values at lower flame speeds using analytical methods [19]. These are used to cover the range of flame speeds seen in the EMERGE experiments. Fig. 15 shows the simplified model results for the methane cases. The nondimensional curves are scaled as defined in Ref. [9], using the energy capacity of the cloud initially within the rig. Both predictions are greater than the experimental data at all locations with the error increasing with flame speed. Fig. 16 shows the propane cases. Again, the simplified method overpredicts at locations in and outside the rig for both flame speeds.

As seen in the *rect* curves of Figs. 12 and 13, the combustion model used by Luckritz contributes to the overprediction. However, here the spherical cloud shape used in the simplified model also plays a part. As Lees [3] highlights, cloud geometries that promote precompression of the unburned gas ahead of the flame generate more severe explosions. The spherical cloud shape is the worst case scenario.

9. Conclusions

CEBAM, the reduced model used here, has been developed incorporating various empirical models to reduce preprocessing and computational time. These reductions are combined with the three-dimensional framework to ensure key factors such as cloud shape, ignition location, cloud migration and blast focusing are included in the VCE analysis. The reduced model has been used to reproduce the earlier results of Luckritz, used in the Baker–Strehlow Method, by employing the same combustion model and cloud shape.

Both the reduced and simplified models are compared to the experimental results of the EMERGE tests. The simplified model overpredicts at all locations due to the assumed cloud shape, the combustion model and neglecting the migration of the cloud outside the rig. The CEBAM model with the decelerating flame speed model can reproduce the experimental results. This increases the confidence in the ability of the model to correctly predict the overpressures from VCE s occurring in process units. The reduced model offers an efficient option for better representation of the actual explosion phenomena with little impact on the efficiency of the analysis process.

Acknowledgements

The authors would like to acknowledge the contributions of Mr. Mike Stahl in development of the CEBAM GUI.

References

[1] K. van Wingerden, O.R. Hansen, P. Foisselon, Predicting blast overpressures caused by vapor cloud explosions in the vicinity of control rooms, Process Safety Progress 18 (1) (1999) 17–24.
[2] B.H. Hjertager, Numerical models of gas explosions (e.g. EXSIM), Proceedings of the Explosion Prediction and Mitigation: Congested Volumes and Complex Geometries, University of Leeds, Leeds, UK, 1997, Nov.
[3] F.P. Lees, Loss Prevention in the Process Industries, 2nd edn., Butterworth-Heinemann, Boston, MA, 1996.
[4] J.K. Clutter, Computation of high-speed reacting flows, PhD Dissertation, University of Florida, 1997.
[5] D.M. Ingram, P. Batten, D.M. Causon, R. Saunders, The representation of small scale obstructions in hydrocode calculations, in: R.J. Perkins, S.E. Belcher (Eds.), Flow and Dispersion Through Groups of Obstacles, Clarendon Press, Oxford, 1997.
[6] J. Warnatz, U. Maas, R.W. Dibble, Combustion, Physical and Chemical Fundamentals, Modeling and Simulation, Experiments, Pollutant Formation, Springer-Verlag, New York, 1995.
[7] R.T. Luckritz, An investigation of blast waves generated by constant velocity flames, PhD Dissertation, University of Maryland, 1977.
[8] R.A. Strehlow, R.T. Luckritz, A.A. Adamczyk, S.A. Shimpi, The blast wave generated by spherical flames, Combustion and Flame 35 (1979) 297–310.
[9] Q.A. Baker, M.J. Tang, E.A. Scheier, G.J. Silva, Vapor cloud explosion analysis, Process Safety Progress 15 (2) (1996) 106–109.
[10] Q.A. Baker, M.J. Tang, E.A. Scheier, G.J. Silva, Vapor cloud explosion analysis, AIChE 28th Annual Loss Prevention Symposium, 1994.
[11] Guidelines for Evaluating the Characteristics of Vapor Cloud Explosions, Flash Fires, and BLEVEs, CCPS, 1994.
[12] W.E. Baker, P.A. Cox, P.S. Westine, J.J. Kulesz, R.A. Strehlow, Explosion Hazards and Evaluation, Fundamental Studies in Engineering vol. 5 Elsevier, 1983.
[13] L.J. Zajac, A.K. Oppenheim, The dynamics of an explosion reaction center, AIAA Journal 9 (1971) 545–553.
[14] T. Echekki, J.H. Chen, Analysis of the contribution of curvature to premixed flame propagation, Combustion and Flame 118 (1/2) (1999) 308–311.
[15] J.H. Lee, C.M. Guirao, K.W. Chiu, G.G. Bach, Blast effects from vapor cloud explosions (1), AIChE Annual Loss Prevention Symposium, 1977.

[16] J.K. Clutter, Use of a reduced combustion model in industrial explosion simulations, AIAA 99-0463, 37th AIAA Aerospace Sciences Meeting, 1999.
[17] J.K. Clutter, W. Shyy, Numerical methods for treating disparate scales in high-speed reacting flows, Numerical Heat Transfer, Part B: Fundamentals 34 (1998) 165–189.
[18] W.P.M. Mercx, N.R. Popat, H. Linga, Experiments to investigate the influence of an initial turbulence field on the explosion process, Final Summary Report for EMERGE, Commission of the European Communities, Contract EV5V-CT93-0274.
[19] R.A. Strehlow, R.T. Luckritz, A.A. Adamczyk, S.A. Shimpi, The blast wave generated by spherical flames, Combustion and Flame 35 (1979) 297–310.